A 1985-2023 time series dataset of absolute reservoir storage in Mainland Southeast Asia (MSEA-Res)

Shanti Shwarup Mahto[1*], Simone Fatichi[1], and Stefano Galelli[2]

[1]Department of Civil and Environmental Engineering, National University of Singapore, 117576, Singapore
5 [2]School of Civil and Environmental Engineering, Cornell University, Ithaca, NY 14853, USA

*Correspondence to: Shanti Shwarup Mahto (ss.mahto@nus.edu.sg)

Abstract

The recent surge in reservoir construction has increased global surface water storage, with Mainland Southeast Asia (MSEA) being a significant hotspot. Such infrastructural evolution demands updates in water management strategies and hydrological
10 models. However, information on actual reservoir storage is hard to acquire, especially for transboundary river basins. To date, no high spatio-temporal dataset on absolute storage time series is available for reservoirs in MSEA. To address this gap, we present (1) a comprehensive, open-access database of absolute storage time series (sub-monthly) for 185 reservoirs (larger than 0.1 km^3) in MSEA spanning the period 1985-2023, and (2) an analysis of the reservoir storage dynamics. The MSEA-Res database includes static (Area-Elevation-Storage curves, water frequency, reservoir extent) and dynamic (area, water level,
15 and absolute storage time series) components for each reservoir. The 185 reservoirs collectively store around 175 km³ (140 km³ – 210 km³) of water, covering an aggregated area of 8,700 km² (6,500 km² – 10,000 km²). We show that the combined average reservoir storage has increased from 70 km³ to 160 km³ (+130%) from 2008 to 2017, primarily contributed by dams in the Irrawaddy, Red, Upper Mekong, and Lower Mekong basins. Our in-situ validation provides a good match between estimated storage and in-situ observations, with 60% of the validation sites (12 out of 20) showing an $R^2 > 0.65$ and an average
20 nRMSE < 15%. The indirect validation (based on altimetry-converted storage) shows even better results, with an $R^2 > 0.7$ and an average nRMSE < 12% for 70% (14 out of 20) of the reservoirs. Furthermore, the analysis of the 2019-2020 drought event reveals that nearly 30-40% of the MSEA region experienced more than five months of drought, with the most significant impact on reservoirs in Cambodia and Thailand. As a result, storage departures ranged up to -40% in some reservoirs, highlighting significant impacts on water availability. Overall, this analysis demonstrates the potential of the inferred storage
25 time series for assessing real-life water-related problems in Mainland Southeast Asia, with the possibility of applications in other parts of the world. The MSEA-Res database and associated Python code are publicly available on Zenodo at https://doi.org/10.5281/zenodo.12787699 (Mahto et al., 2024).

1 Introduction

Water reservoirs cause some of the most significant human-induced alterations of the hydrological cycle, influencing the re-
30   distribution of water in space and time (Chao et al., 2008; Cooley et al., 2021; Haddeland et al., 2014; Lehner et al., 2011).
The construction of reservoirs can also lead to significant environmental and socio-economic impacts, including biodiversity
loss, alterations of geochemical cycles, and changes in land use patterns (Degu et al., 2011; Kirchherr et al., 2016; Maavara et
al., 2020; Vörösmarty et al., 2010; Winemiller et al., 2016). Despite these impacts, reservoirs remain pivotal in generating
renewable energy and supporting water management, thus driving the demand for new dams (Chao et al., 2008; Wada et al.,
35   2017), especially in the Global South. Accurate information on reservoir operations is thus crucial for practitioners,
policymakers, and scientists to estimate water budgets, assess hydrological and nutrient fluxes, project water availability for
hydropower generation, and mitigate flood and drought risks (Bakken et al., 2014; Chao et al., 2008). Information on the
temporal evolution of *absolute* reservoir storage, or level, is particularly useful, since it provides a direct measurement of the
total volume of water stored in a reservoir at any given time – this contrast against *relative* storage time series, which only
40   track changes in storage across a given time interval.

Currently, information on long-term absolute reservoir storage is limited across most of the globe, with consolidated datasets
available only for a handful of countries (Steyaert et al., 2022; Li et al., 2023; Steyaert and Condon, 2024). Such type of
information is particularly needed in regions – like Mainland Southeast Asia – that are experiencing rapid hydropower
45   development. Laos, for instance, is realising its vision of becoming the "Battery of Asia" by constructing new hydropower
dams and exporting electricity to neighbouring countries; it is expected, moreover, that several additional dams will become
operational in the years to come (Ang et al., 2024). Similarly, other Southeast Asian countries, such as Vietnam and Cambodia,
have also built most of their reservoirs in the past two decades (Ang et al., 2024; Zhang and Gu, 2023), altering the flow of
transboundary rivers and raising tensions between countries. With this concern in mind, we focus on the reservoirs of Mainland
50   Southeast Asia, thus comprising Myanmar, Thailand, Laos, Vietnam, Cambodia, Malaysia, Singapore, and part of southern
China – where a few large rivers flowing in the region originate.

The problem of inferring reservoir storage time series can only be partially addressed with the aid of hydrological models,
since some basic information on operational strategies – typically not available – is needed to setup and validate models (Zhang
55   et al., 2014; Dang et al., 2020; Galelli et al., 2022; Nazemi and Wheater, 2015a, b; Vu et al., 2022; Wada et al., 2017).
Fortunately, advances in remote sensing offer a viable opportunity to estimate storage by relating information on reservoir
surface area and elevation (Busker et al., 2019; Gao et al., 2012; Tortini et al., 2020; Vu et al., 2022). For this task, information
on reservoir bathymetry – synthesized by Area-Elevation-Storage (A-E-S) curves – becomes crucial. It is indeed common
practice to derive the A-E-S curves from remotely-sensed digital elevation models (DEMs) (Zhang and Gao, 2020); their time
60   of acquisition, however, may limit the available information. When the DEM captures the reservoir's topography before its

filling begins, absolute storage estimation is possible using these remotely sensed data (Li et al., 2023). For reservoirs constructed before the DEM was made available, the problem lies in the fact that satellite-based DEMs do not provide information below the reservoir water surface, leading to a partially unknown bathymetry. However, even in such cases, remotely sensed water surface area from sensors like Landsat, Sentinel, and MODIS, or water level data from satellite

65   altimeters such as JASON, Sentinel-6, and SARAL-Altika, can still be used to estimate storage changes (Das et al., 2022; Minocha et al., 2024; Zhang et al., 2014). Therefore, while recent studies have quantified long-term surface area and storage changes of reservoirs at global (Busker et al., 2019; Hou et al., 2024; Tortini et al., 2020) and regional scales (Shen et al., 2023; Song et al., 2022), absolute storage estimations – especially for those reservoirs built before 2000 (acquisition year of SRTM DEM) – are still uncertain in space and time because of the lack of detailed bathymetry information (Hao et al., 2024; Li et al.,

70   2023; Zhang and Gao, 2020).

How to improve such estimates? Radar altimetry has proven useful for measuring water levels in lakes and reservoirs (Markert et al., 2019; Schwatke et al., 2015; Vu et al., 2022). Yet, limited coverage is a major limitation in popular altimetry-based datasets, such as Hydroweb (Crétaux et al., 2011), G-REALM (Birkett et al., 2011), and DAHITI (Schwatke et al., 2015). For

75   Mainland Southeast Asia, altimetry-based water level data are available for only a few (20-30) reservoir overpasses. On top of that, the available water level datasets are not continuous in time. Although time series datasets are available for reservoir storage anomaly (Shen et al., 2022, 2023), none of them provide long-term time series for absolute reservoir storage. Some studies modelled total storage – only for a few reservoirs – using LiDAR data (Bacalhau et al., 2022; Chen et al., 2022; Li et al., 2020), surrounding topographical information (Fang et al., 2023; Liu et al., 2020; Liu and Song, 2022), or through

80   simplified modelling approaches (Khazaei et al., 2022; Yigzaw et al., 2018). However, they show inaccuracies in storage estimates for reservoirs that were built before 2000, because of the (necessary) assumptions on reservoir bathymetry (Hao et al., 2024; Li et al., 2023; Zhang and Gao, 2020). Other studies relied on field surveys to create three-dimensional (3D) bathymetry maps to estimate absolute storage, but these are limited to very few reservoirs (Busker et al., 2019; Weekley and Li, 2019).

85

Recently, the GloLakes database was produced by Hou et al., (2024), providing absolute water storage dynamics for lakes from 1984 to 2020 - for 27,000 global lakes and reservoirs using the geostatistical model described in Messager et al., (2016). Although it covers the entire globe by providing a comprehensive dataset for large-scale assessments, it has a few limitations for the reservoirs located in Mainland Southeast Asia. First, the model parameters (used in the storage estimation) strongly

90   depend on mean depth (extrapolating the surrounding topographical slope towards the centre of the lake to estimate lake depth), the surface area of the lake (derived from Landsat satellite images), and average slope (derived from DEM). Therefore, uncertainties in the estimates of reservoir storage may be generated by the estimation of depth, slope, and through other model coefficients. Second, GloLakes does not include some of the largest reservoirs in MSEA, including Nuozhadu (22 km^3),

Xiaowan (15 km^3), Xe Kaman 1 (4 km^3), and Lower Seasan 2 (6 km^3), which play a significant role in water redistribution

95   and hydropower generation (Ang et al., 2024; Galelli et al., 2022; Vu et al., 2022).

Here, we address these gaps by presenting a robust and comprehensive sub-monthly time series dataset of absolute reservoir storage for Mainland Southeast Asia (hereafter, "MSEA-Res database"), whose reservoir network is described in Section 2. Specifically, our open-access database includes sub-monthly time series data of absolute storage for 185 reservoirs (larger than

100   0.1 km^3) in mainland Southeast Asia (MSEA), covering the period from 1985 to 2023. The creation of this database is facilitated by two technical advances (Section 3), namely (1) the concomitant use of Landsat and Sentinel-2 images, and (2) the creation of hypsometric curves based on the new database introduced by Hao et al., (2024), which provides bathymetry information for all dams in the GRanD database. The first advancement is aimed to increase the temporal resolution of our time series, while the latter allows us to address the (aforementioned) challenges concerning the estimation of hypsometric

105   curves for dams that were not recently built. To demonstrate the usefulness of MSEA-Res, we conduct a multi-basin analysis of the dynamics and trends of reservoir (absolute) storage, offering insights into how storage patterns have evolved over the years and across different basins (Section 4). Finally, we analyse the impact of the 2019-2020 drought on surface water storage, highlighting the significant effects of extreme dry weather events on water resources in Mainland Southeast Asia. Through these examples, we show that MSEA-Res can be used for a variety of applications, such as hydrological modelling, drought

110   analyses, and regional water resources planning.

2 Water reservoirs in Mainland Southeast Asia

2.1 Dam design attributes

We first analysed global and regional dam databases to compile a list of reservoirs (with storage larger than 0.1 km^3) built in Mainland Southeast Asia until 2023. As shown in Table 1, we used two global databases [GRanD Version-1.3 (Lehner et al.,

115   2011) and GDAT (Zhang and Gu, 2023)] and one regional database for the Mekong (Ang et al., 2024). The most popular global dam database – GRanD – was used to get the list of georeferenced dams that were built until 2016. Unfortunately, the GRanD database has not been updated for post-2017 dams in our study region. Therefore, we collected the list of georeferenced dams built between 2017 and 2023 from more recent databases. For the Mekong basin, we used the dam database prepared by Ang et al., (2024), whereas the GDAT database was used for the other basins (i.e., Chao Phraya, Red, Salween, Irrawaddy,

120   and remaining smaller river basins). Information on each reservoir in the final list of 185 elements was verified and validated against high-resolution Google Earth images. Among the reservoir attributes, we collected four main ones: name of the reservoir, spatial coordinates of the dam (i.e., longitude and latitude), storage capacity, and year of commission.

Table 1. List of global and regional dam databases used to collect the dam design attributes.

Category	Database	Region	Number of dams	Period	Source
Global	GRanD v1.3 (https://ln.sync.com/dl/bd47eb6b0/anhxaikr-62pmrgtq-k44xf84f-pyz4atkm/view/default/447819520013/)	Mainland Southeast Asia	125	Until 2016	Lehner et al., 2011
	Global Dam Tracker (GDAT) (https://zenodo.org/records/7616852/)	Mainland Southeast Asia, except the Mekong	22	2017-2023	Zhang and Gu, 2023
Regional	Dams in the Mekong (https://doi.org/10.21979/N9/ACZIJN/)	Mekong basin	38	2017-2023	Ang et al., 2024

2.2 Distribution and evolution of reservoirs

Based on the acquired information, we first present the distribution and temporal evolution of reservoirs in Mainland Southeast Asia (Fig. 1). Among the 185 large reservoirs in MSEA, 125 (~68 %) were built in the twenty-first century. As a result, a dense network of newly constructed reservoirs spreads across all basins, with the exception of the Chao Phraya, western Lower Mekong, and southern coastal basins (Fig. 1a). The first big reservoirs (mainly, Srinagarind - 18 km^3, Kenyi - 13.6 km^3, Bhumibol - 13.5 km^3, Sirikit - 9.5 km^3, Khao Laem - 8.8 km^3, and Nam Ngum - 7.0 km^3) were built between 1964 and 1985, increasing the aggregated storage capacity from 0 to ~75 km^3 in about twenty years (Fig. 1c). During the following 15 years (1986-2000), mostly small reservoirs were constructed, except for Rajjaprabha (5.6 km^3), which started to operate in 1987. Until 2000, the cumulative storage from 60 reservoirs in Mainland Southeast Asia was thus ~85 km^3. The construction of 125 new reservoirs in the post-2000 period sharply increased the aggregated water storage by more than two-fold, reaching a storage capacity of ~180 km^3 at the end of 2023 (Fig. 1c). During this time, a few mega reservoirs were built, such as Xiaowan (~15 km^3) and Nuozhadu (~22 km^3) in the Upper Mekong basin, contributing significantly to the aggregated storage capacity of Mainland Southeast Asia. At present, the largest number of reservoirs is in the Lower Mekong River basin (54), followed by the Irrawaddy (29), Red River (21), Upper Mekong (20), Chao Phraya (7), and Salween (3) [Fig. 1b, d]. 51 dams are located in the remaining river basins (Indicated as "Others" in Fig. 1b, d). Although, based on the design specifications, we know how much water the reservoirs can hold, when full, we need a database containing time series of reservoir storage to better support hydrological studies and water resources management. Our MSEA-Res fills this gap.
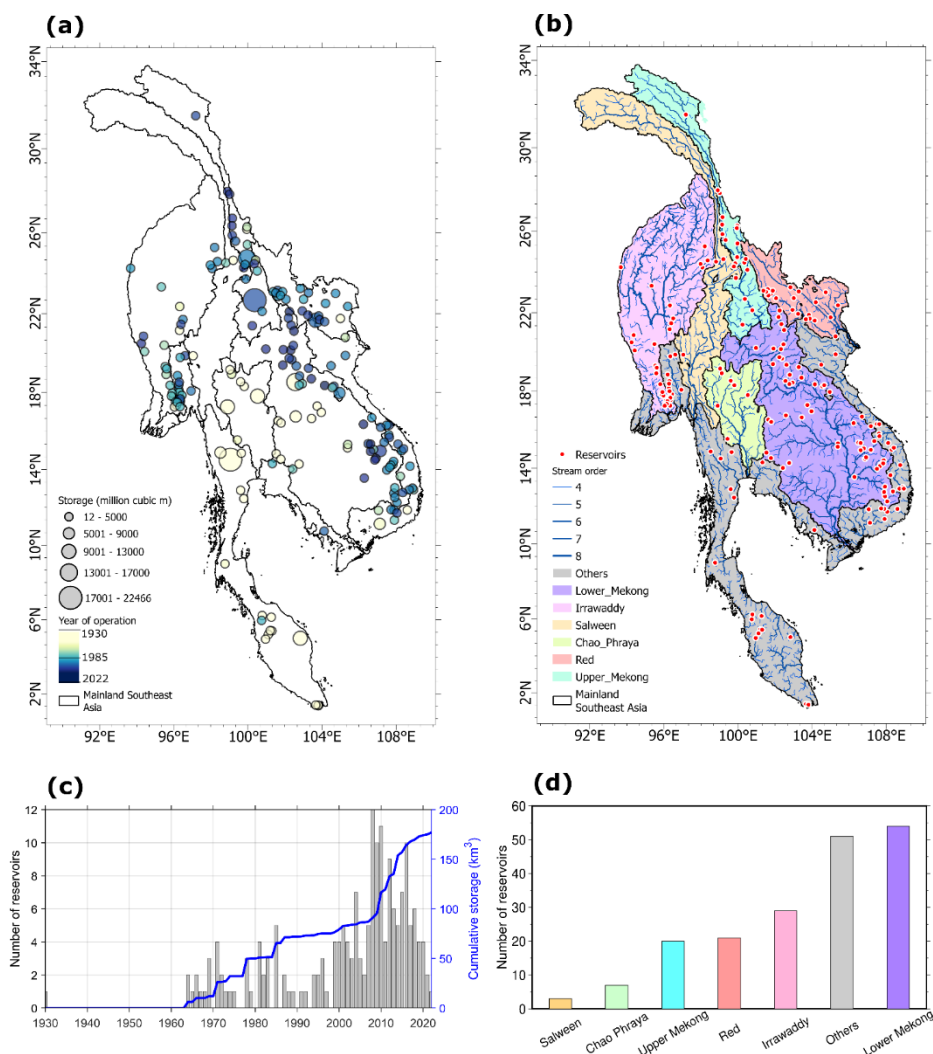
Figure 1: Spatial distribution and evolution of reservoirs in Mainland Southeast Asia. (a) Map showing reservoir storage volume
(million m³), where the size of the circle is proportional to the reservoir capacity while the colour represents the year of commission
of the dams. (b) Basin-wise distribution of dam location (red dots), stream network, and order. (c) Number of dams built per year
and their corresponding cumulative storage capacity. (d) Basin-wise total number of reservoirs built until 2023.

3 Methodological framework

The procedure adopted to produce the MSEA-Res database is illustrated in Fig. 2 and can be divided into three main steps. For
each reservoir, we first derive the Area-Elevation-Storage relationship (i.e., A-E curve, E-S curve, and A-S curve), then we
calculate the time series of water surface area, and finally, we derive the absolute reservoir storage by combining information
on the reservoir surface area (or water level, if available) with the hypsometric curves. Although water levels from satellite
altimetry observations can also be used to estimate the storage volume (Zhang et al., 2014), they are only available for a few
reservoirs, and they are neither consistent nor continuous in time, thus creating missing data issues (Birkett et al., 2011; Busker

155 et al., 2019; Schwatke et al., 2015). Therefore, we worked with satellite-based water surface area, which can be produced at higher frequency (e.g., sub-monthly) from the Earth Observation Satellites, such as Landsat and Sentinel-2, to retrieve the reservoir's area time series. In the following sub-sections, we discuss each step-in detail, namely acquiring the raw satellite data, obtaining the hypsometric curves for different reservoirs, estimating water surface area, improving the area estimates, and finally inferring the storage time series. All steps are implemented in a Python package called *InfeRes* (publicly available

160 on GitHub, https://github.com/Critical-Infrastructure-Systems-Lab/InfeRes/).
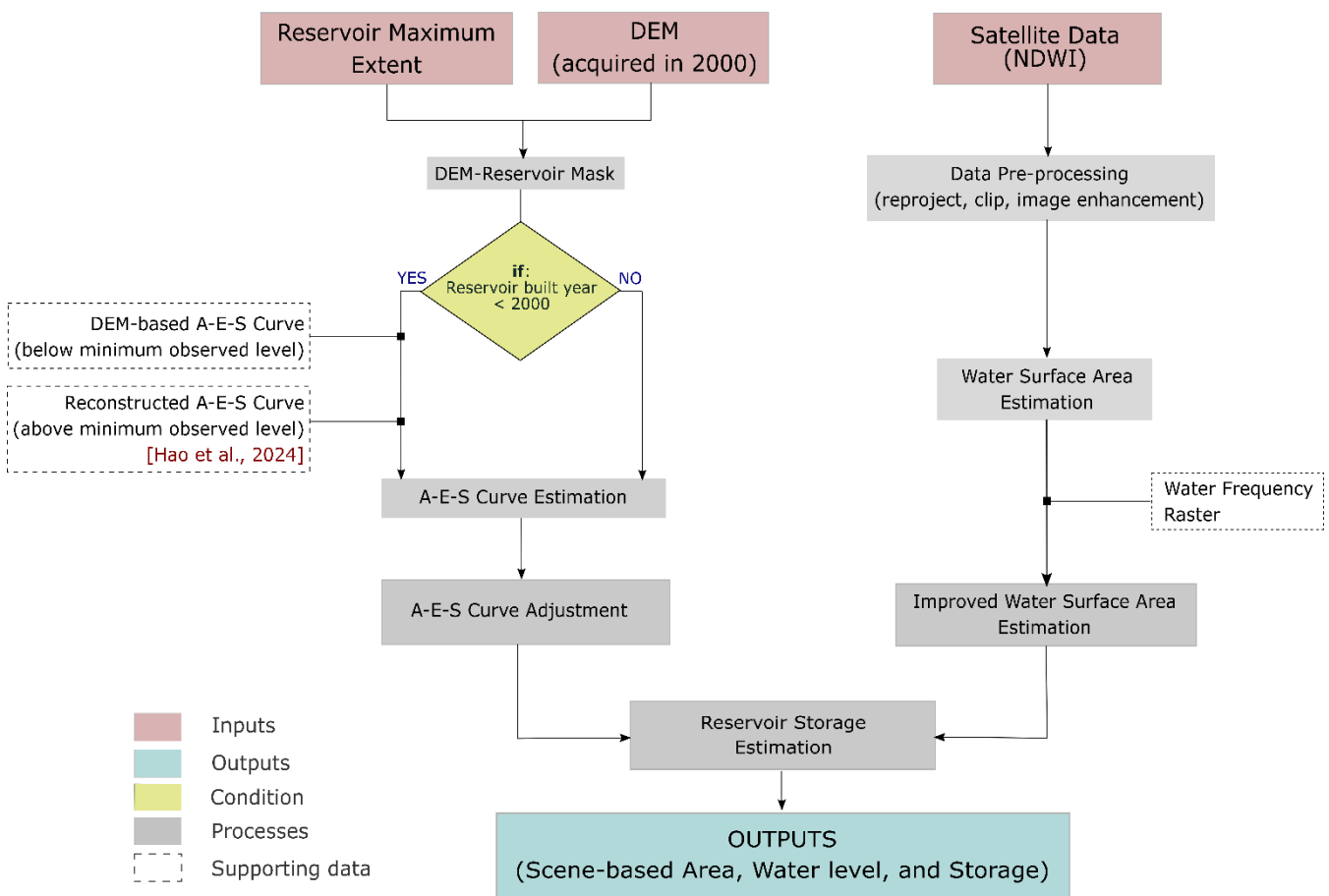
Figure 2: Flowchart showing the methodological framework and steps taken to estimate reservoir storage from time series satellite
165 **images. DEM is the 30m digital elevation model from the SRTM, acquired in February 2000. Normalized Difference Water Index (NDWI) is the normalized ratio between reflectance in Green and NIR bands, given by (Green-NIR)/(Green+NIR), which is generally used to classify water and non-water pixels.**

3.1 Acquiring input data

170 The process starts by acquiring the input datasets, mainly the Digital Elevation Model (DEM), Normalized Difference Water Index (NDWI) images, Water Frequency raster (FREQ), and Maximum Water Extent raster (EXT). We used the Google Earth Engine (GEE) coding platform to acquire the necessary input dataset. For each reservoir, rectangular bounding boxes are used to fix the dimension of the dataset in the GEE. As for the digital elevation model, we used the Shuttle Radar Topography Mission (SRTM, Farr et al., 2007) DEM-Version3, an international research effort that obtained digital elevation models on a near-global scale. NASA JPL provides the SRTM V3 product at a resolution of 1 arc-second (~30m). Unlike the DEM, the

175 other maps (NDWI, FREQ, and EXT) were estimated from the Landsat-5 TM, Landsat-7 ETM+, Landsat-8 OLI/TIRS, Landsat-9 OLI-2/TIRS-2, and Sentilel-2 images (see Table 2 for details).

Table 2. List of input satellite data and their specifications.

Category	Database	Availability	Resolution	Earth Engine Snippet
DEM	SRTM DEM V3	2000	30m	ee.Image("USGS/SRTMGL1_003")
Landsat	Landsat-5 TM	1984-2012	30m	USGS Landsat 5 Level 2, Collection 2, Tier 1 ee.ImageCollection("LANDSAT/LT05/C02/T1_L2")
	Landsat-7 ETM+	1999-Present	30m	USGS Landsat 7 Level 2, Collection 2, Tier 1 ee.ImageCollection("LANDSAT/LE07/C02/T1_L2")
	Landsat-8 OLI/TIRS	2013-Present	30m	USGS Landsat 8 Level 2, Collection 2, Tier 1 ee.ImageCollection("LANDSAT/LC08/C02/T1_L2")
	Landsat-9 OLI-2/TIRS-2	2021-Present	30m	USGS Landsat 9 Level 2, Collection 2, Tier 1 ee.ImageCollection("LANDSAT/LC09/C02/T1_L2")
Sentinel	Sentinel-2	2016-Present	30m (resampled)	Harmonized Sentinel-2 MSI: MultiSpectral Instrument, Level-1C ee.ImageCollection("COPERNICUS/S2_HARMONIZED")

180 The Green (G) and Near-infrared (NIR) bands from the satellite sensors (Landsat and Sentinel) are used to calculate NDWI [i.e. (G-NIR)/(G+NIR)] – as proposed by McFeeters, (1996) – for the available scenes, collectively covering the study period 1985-2023. Optical images (G and NIR) can be affected by the presence of clouds – especially on rainy days – and so, NDWI. Therefore, getting a complete view of reservoir extent from a cloud-affected NDWI image becomes significantly challenging (Hou et al., 2024; Vu et al., 2022). To address this issue, we first filtered the Earth Engine Image Collection based on cloud

185 threshold (Band Quality, BQ) and selected only those images that have less than 80% cloud coverage. We also made NDWI composites from available Landsat (1985-2023) and Sentinel (2016-2023) images at 10-day intervals. Therefore, one month can have a maximum of three images (i.e., only from Landsat) during the period 1985-2015. On the other hand, it can have a maximum of six images per month (three from Landsat and three from Sentinel) in 2016-2023. Making a composite of NDWI images maximizes the chances of getting more cloud-free pixels than individual NDWI images.

190   To obtain the water frequency (FREQ) and maximum water extent (EXT) raster maps, we first create the binary NDWI images available between 2013 and 2023 from the Landsat and Sentinel image collection in the GEE environment. Positive NDWI values are considered an approximation for water pixels (with a value of 1), while negative NDWI values are non-water pixels (with a value of 0). The FREQ layer is created by making a composite of all binary NDWI images whose cloud percentage is less than 20% (i.e., clear sky condition) and by dividing it by the total number of selected images (cloud percentage <20%).

195   We multiply the FREQ layer by 100 to get the percentage of water present at each pixel. Subsequently, the EXT layer is created by simply taking the largest extent of ones in all binary NDWI images available between 2013 and 2023. Overall, we assemble three raster layers (DEM, FREQ, and EXT) and scene-based NDWI images for each of the 185 reservoirs, which we process further to estimate the absolute reservoir storage time series.

3.2 Area-Elevation-Storage curves

200   Deriving the relationship between the area, elevation (or water level), and storage (A-E-S relationship) of a reservoir is crucial. This step relies on the bathymetry information, which further depends on the time of acquisition of the DEM. Considering that the SRTM-DEM was acquired in February 2000, reservoirs built after 2000 have complete bathymetry information; thus, the A-E-S relationship for the year 2000 can easily be derived. Since the majority of the reservoirs (~70%) in Mainland Southeast Asia were built after 2000, we obtained the Area-Elevation-Storage (A-E-S) curves from the DEM. For each reservoir, the

205   elevation range for the A-E-S curves was defined by the minimum and maximum DEM values within the reservoir's extent. The area at each elevation level was determined by contouring, while the corresponding absolute storage was estimated by cumulatively summing the areas across the elevation range. For the remaining 30% of the reservoirs built before 2000, the DEM cannot be applied directly to estimate E-A-S curves. This is a common problem in the existing studies for estimating absolute storage for reservoirs built before 2000 (Busker et al., 2019; Gao et al., 2012; Hou et al., 2024; Khazaei et al., 2022;

210   Yigzaw et al., 2018). Although previous studies have used various modeling approaches based on simplified geometric assumptions to overcome this limitation (Fang et al., 2023; Hou et al., 2024; Khazaei et al., 2022; Yigzaw et al., 2018), results often do not meet the level of accuracy required for basin-scale water management modeling and decision-making. To address this problem, we banked on a recently-released database of global reservoir area-storage-depth derived through deep learning-based bathymetry reconstruction (GRDL; Hao et al., (2024)), which provides reliable bathymetry information for the 7,250

215   GRanD reservoirs across the globe. We thus utilized the GRDL database to obtain A-E-S curves for the remaining 60 reservoirs (Fig 2).

3.3 Water surface area estimation

We used the Landsat and Sentinel-based NDWI images downloaded from the Google Earth Engine platform (see section 3.1 for details) to estimate the reservoir water surface area. A locally-adjusted Contrast Limited Adaptive Histogram Equalization

220   (CLAHE) was applied to enhance the NDWI images before classification. CLAHE (Reza, 2004) is a variant of Adaptive histogram equalization (AHE), which takes care of over-amplification of the contrast in an image. CLAHE operates on small

regions in the image (8 x 8 pixels window in our case) rather than the entire image. We then applied the *k*-means clustering-based algorithm to classify the water pixels. We assigned a number of clusters (*k*) equal to three to classify each NDWI image to represent three different classes, i.e., water, non-water, and no data. Because of the presence of clouds and other disturbances,

225 using the same NDWI threshold (equal to 0) in all satellite images may lead to overestimation or underestimation errors of the water surface area (Vu et al., 2022). Thus, to find NDWI thresholds for each satellite image, we resort to *k*-means clustering. Eventually, the preliminary water pixels were identified by selecting the cluster corresponding to the maximum centroid value of NDWI.

230 We further improved the water surface area estimates by filling the cloud-contaminated pixels, which were assigned a "No Data" value in the previous steps. To this purpose, we used the algorithm for water surface area estimation developed by Vu et al., (2022), which was initially introduced by Gao et al., (2012) and Zhang et al., (2014) to extract water surface area. The algorithm uses a water frequency raster (FREQ) to fill the cloud-affected pixels over the reservoir area. Finally, we add the clear water pixels (*k*-means clustering) and cloud-filled water pixels (Vu et al., 2022) to get a complete picture of the reservoir

235 water surface area for each NDWI image.

3.4 Absolute storage estimation and post-processing

Once estimated the water surface area, we subsequently used the hypsometric curves to derive the corresponding absolute reservoir storage volume. Based on different processing stages, we post-processed the storage time series into three levels (Level-0, Level-1, and Level-2). For each reservoir, Level-0 corresponds to the scene-based (instantaneous) raw outputs of

240 absolute reservoir storage, which have been derived from the available satellite images. We then performed a simple box plot analysis on Level-0 data to remove the outliers, creating the so-called Level-1 data. Note that these data are created using a generalized box-plot framework for quality control that is not specifically designed for each reservoir; therefore, on a case-to-case basis, some values in the storage time series may still be considered outliers—which can be removed manually or with the aid of other data analysis algorithms. Considering the demand for ready-to-use data for several applications (e.g.,

245 hydrological modelling), we further processed the Level-1 data to create continuous daily time series of absolute reservoir storage (called Level-2 data) using a trend-preserving interpolation technique, followed by data smoothening (moving mean method). It is important to note that the interpolation technique incorporates all available data points, including a few outliers, which introduces a higher level of uncertainty in the Level-2 data. Despite this, we undertook validation of the storage time series to strengthen confidence in our estimations.

3.5 Validation of reservoir storage

250

We adopted two validation approaches. The first approach is direct validation, where we compare and validate our estimated storage volume against observed reservoir storage. The second is indirect validation, where we use altimetry-converted storage to validate our time series of reservoir storage. Acquiring observed reservoir storage is challenging in MSEA because of the

institutional and organizational data-sharing policies and restrictions, leading to a poor network of public data repositories for

255 reservoir data. The only exception is the Thailand National Hydroinformatics Data Centre, which releases daily reservoir storage information to the public domain (National Water Database (NWD) - https://www.thaiwater.net/). We took the opportunity to download observed storage data from the NWD portal for 20 reservoirs in Thailand, and then compared these data with our storage estimates.

260 For indirect validation, we used reservoir water level data measured by satellite-based altimeters such as TOPEX/Poseidon; Jason-1, Jason-2, and Jason-3; ENVISAT; ERS-1 and ERS-2; and Sentinel-3 and Sentinel-6, which have proven useful in measuring water levels in lakes and reservoirs (Birkett, 1998; Frappart et al., 2006; Santos da Silva et al., 2010). Specifically, we acquired the compiled time series of radar-altimetry-derived surface water elevation from the Database for Hydrological Time Series of Inland Waters (DAHITI- https://dahiti.dgfi.tum.de/) (Schwatke et al., 2015), and the Global Reservoirs and

265 Lakes Monitor (GREALM- https://ipad.fas.usda.gov/cropexplorer/global_reservoir/) (Birkett et al., 2011). We took 20 reservoirs across Mainland Southeast Asia – for which altimetry observations are available – to indirectly validate our estimated storage time series. Before carrying out the comparison, the altimetry-derived surface water levels were first converted to their corresponding storage time series based on the Elevation-Storage relationship.

4 Results

270 ### 4.1 Structure of the MSEA-Res database

The reservoir's information in the database is divided into static and dynamic components (Figure 3 and Table 3). For each reservoir, static information is further divided into four categories: i) Area-Level-Storage relationship (hypsometric curves), (ii) reservoir extent, iii) water frequency (mean inundation frequency for each pixel), and iv) reservoir's characteristics such as location (longitude and latitude), year of commission, area (km^2), water level (m), and storage (million m^3). Note that for

275 area, level, and storage, static information includes minimum, mean, and maximum. On the other hand, dynamic information consists primarily of the sub-monthly time series of absolute reservoir storage. We did not separately provide the water-level and surface area time series, as they can easily be derived from the Area-Level-Storage curve for any given storage volume. In the subsequent sections, we use Level-1 and Level-2 data to analyze and validate the storage time series. Note that, for each reservoir, the data are processed within the period 1985-2023. If the year of commission of a reservoir is 2015, then the storage

280 time series is estimated between the years 2010 and 2023, assuming a maximum of five years as the filling period. All storage time series and other related information are publicly available in the MSEA-Res database at https://doi.org/10.5281/zenodo.12787699 (Mahto et al., 2024).

Mainland Southeast Asia's water reservoirs
(MSEA-Res) catalogue

Static components

♦ **Area-Level-Storage relationship** (curves)

♦ **Reservoir extent** (georeferenced raster image)

♦ **Water frequency** (georeferenced raster image)

♦ **Reservoir's characteristics** (location, year of commission, area, water level, and absolute storage

Dynamic components
(Storage time-series)

♦ **Level-0:** Scene-based raw outputs

♦ **Level-1:** Scene-based filtered outputs (outliers removed)

♦ **Level-2:** Continuous daily outputs (interpolated and smoothened)

285   **Figure 3: Catalogue of the MSEA-Res database. Please note that the dynamic components (storage time series) are available from five years before the year of commission.**

Table 3. Reservoir attributes in the MSEA-Res database.

Category	Datatype	Attributes	Description
Static components	Area-Level-Storage relationship	Level_m_	Water level
		Area_sq_km_	Water surface area (empty reservoir)
		Storage_mcm_	Absolute storage (empty reservoir)
	Reservoir extent		Georeferenced image (.TIFF)
	Water frequency		Georeferenced image (.TIFF)
	Reservoir's characteristics	Sl_No	Serial number as per MSEA-Res database
		GRAND_ID	Identification number in the GRanD database (Lehner et al., 2011). For a non-GRandD reservoir, the value is 9999.
		Longitude	Longitude in degrees decimal
		Latitude	Latitude in degrees decimal
		Year_of_commission	Year of commission of the reservoir
		Area_min_sqkm	Minimum water surface area (km^2)
		Area_avg_sqkm	Average water surface area (km^2)
		Area_max_sqkm	Maximum water surface area (km^2)
		WL_min_m	Minimum surface water level (m)
		WL_min_m	Average surface water level (m)

		WL_min_m	Maximum surface water level (m)
		Storage_min_mcm	Minimum water storage (million m^3)
		Storage_min_mcm	Average water storage in (million m^3)
		Storage_min_mcm	Maximum water storage in (million m^3)
Dynamic components (Storage time series)	Level-0	ID	Satellite data identification number (L0= Landsat and S2= Sentinel)
		Date	Image collection data
		Cloud_percentage	Percentage of cloud cover over the reservoir
		Quality	Quality control indicator (1= Good, 0= Bad)
		Before_area	Instantaneous water surface area before improvement (km^2)
		After_area	Instantaneous water surface area after improvement (km^2)
		Final_area	Instantaneous water surface area after final check (km^2)
		dem_value_m	Instantaneous surface water level (m)
		Tot_res_volume_mcm	Instantaneous water storage after a final check (million m^3)
	Level-1	Same as Level-0	Same as Level-0
	Level-2	Date	Daily dates
		Storage_mcm	Interpolated instantaneous water storage (million m^3)

4.2 Hypsometric curves and storage time series

290   In this section, we illustrate one of the static components of the MSEA-Res database, i.e., the Area-Elevation-Storage relationship (see Table 3 for details), where elevation corresponds to the reservoir's water level relative to mean seal level in meters (m a.s.l). In our database, we provide the hypsometric curves for each of the 185 reservoirs. Here, we further illustrate seven curves (Fig. 4); one reservoir for each major river basin. The seven selected reservoirs (basin) are Longjiang (Irrawaddy), Nuozhadu (Upper Mekong), Son La (Red), Mobye (Salween), Sirikit (Chao Phraya), Sringarind (Other basins), and Xe

295   Kaman1 (Lower Mekong). The Area-Elevation (A-E curve) and Storage-Elevation (S-E curve) relationships are shown (Fig. 4). These hypsometric curves represent the variability in reservoir's storage and area, which results primarily from the diverse topography characterising the basins and dam locations.

For the same seven reservoirs, we then illustrate the dynamic components of the MSEA-Res database – time series of reservoir

300   storage at different processing levels, i.e., Level-0 (raw outputs), Level-1 (removal of outliers from Level-0), and Level-2 (smooth interpolation of Level-1) (Fig. 5). The storage time series data can be used to infer meaningful information on the storage dynamics, including filling patterns, fluctuations, and response to wet and dry years. Looking at the filling patterns, for instance, Xe Kaman1 (2016) took almost four years to store more than 3 km^3 of water and reach its normal operating

conditions (Fig. 5g). The Longjing (2010) reservoir was filled in roughly one year (Fig. 5a). By combining this information
305 with inflow data, one could easily estimate the impact of reservoir filling strategies on downstream water availability—a rather
contentious matter in transboundary river basins (Vu et al., 2022; Wheeler et al., 2016; Zaniolo et al., 2021). The time series
also reveal the 'typical' behaviour of reservoir storage in Southeast Asia, with seasonal fluctuations between minimum and
maximum operating levels driven by the drastic changes in the intra-annual water availability characterizing this region (i.e.,
a wet season between June and November followed by a drier period between December and May) (Nguyen et al., 2020).
310 Importantly, the time series also reveal inter-annual changes in water storage, which are largely caused by hydrological-regime
variability – a point further discussed in Section 4.5.
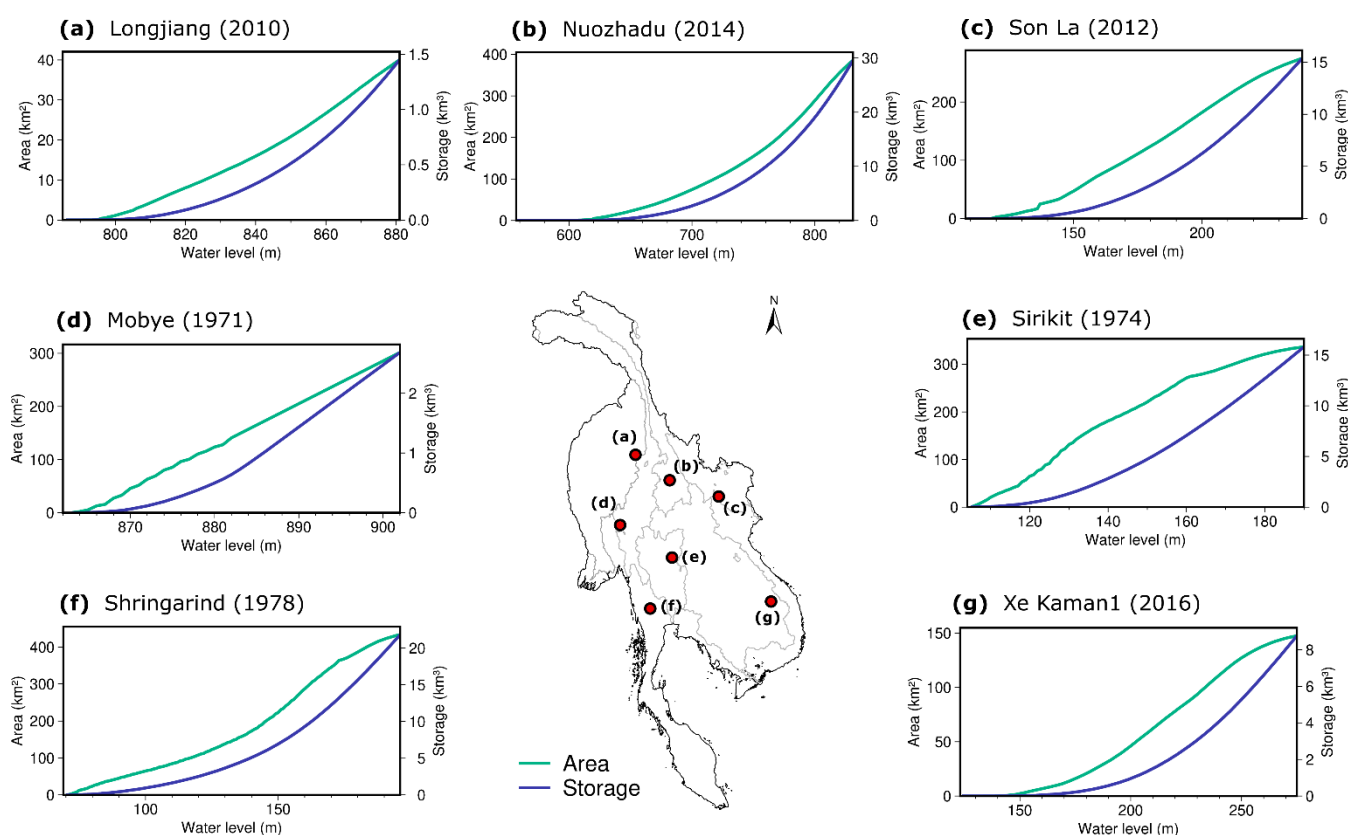
315 **Figure 4: Illustration of the static components of MSEA-Res database (Area-Elevation-Storage relationship) for seven reservoirs,
one in each of the major river basins, based on their maximum storage capacity. In each panel, Elevation-Area (E-A) and Elevation-
Storage (E-S) curves are shown in green and blue, respectively. The dates refer to years of completion of the reservoirs.**
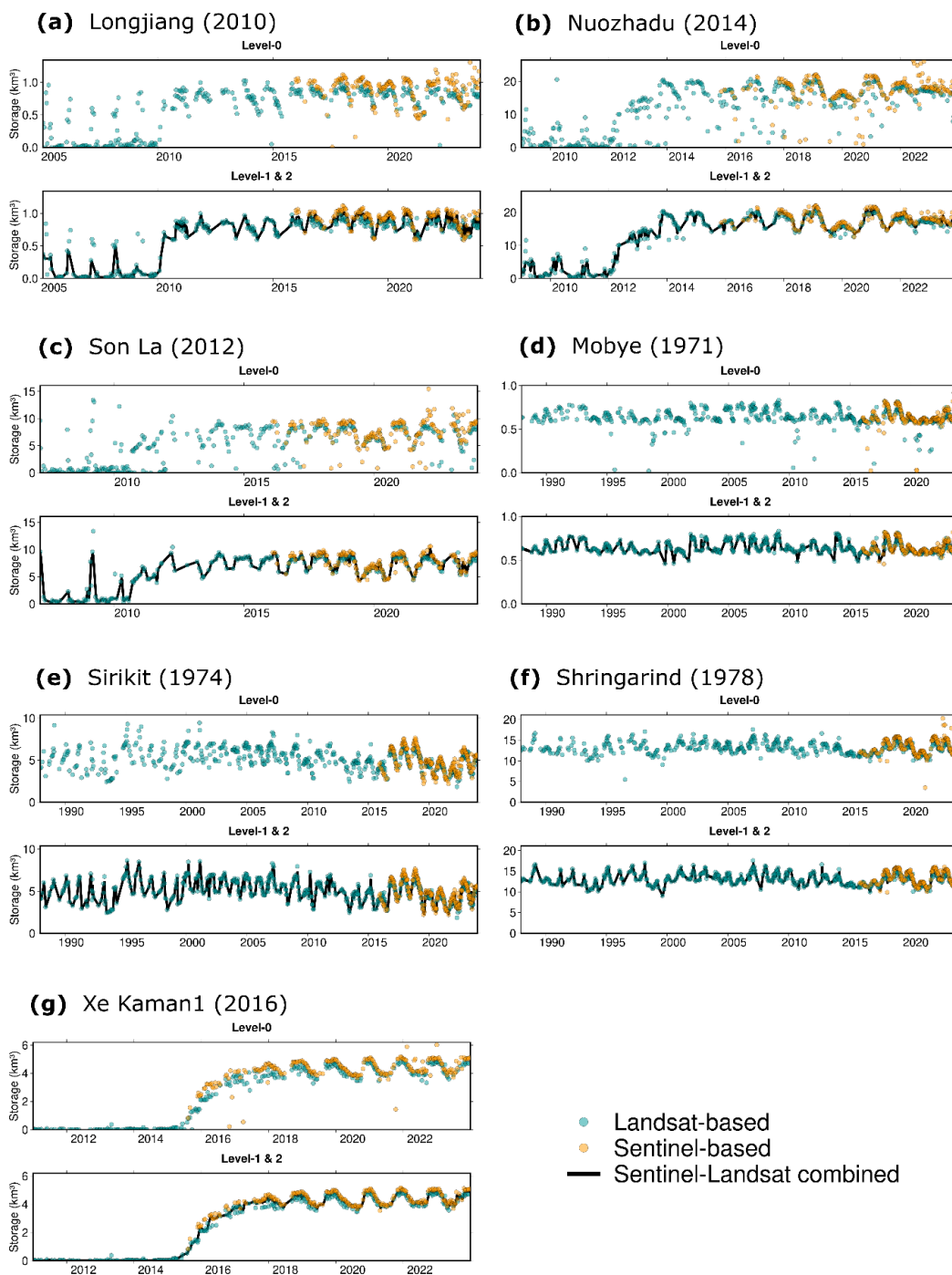
Figure 5: Illustration of reservoir storage time series – i.e., the dynamic components of the MSEA-Res database, for the seven selected reservoirs. Each panel (a-g) corresponds to a reservoir. For each panel, we report the scene-based reservoir storage (km³)

time series at Level-0, and the storage time series at Level-1 (after removing the outliers) overlapped with Level-2 (after interpolation and smoothening).

325

4.3 Basin-wise reservoir storage analysis

We used all Level-1 data to analyse the basin-wise evolution and dynamics of reservoir storage in Mainland Southeast Asia. Specifically, we calculated the total volume of water (km^3) stored in all reservoirs for each of the main seven river basins, namely Irrawaddy, Upper Mekong, Red, Salween, Chao Phraya, Lower Mekong and "other basins" lumped together (Fig. 6).

330   We found that the aggregated storage of all reservoirs in the Upper Mekong basin has increased by more than eight times (800% increase) in just five years (between 2010 and 2015) (Fig. 6b). Nuozhadu (22 km^3) and Xiaowan (15 km^3) are the main contributors to such increase, as they account approximately for 95% of the basin-total storage, whereas the remaining 18 reservoirs contribute just 5% (Fig. 6b). Since the construction of Nuozhadu and Xiaowan, more dams have been built in the Upper Mekong; yet, their capacity is smaller than the one of these two mega dams (e.g., Miaowei, 0.66 km^3). A seasonal

335   fluctuation of storage is common across all basins, as the monsoon season has a similar precipitation pattern across the MSEA region (Ha et al., 2023; Skliris et al., 2022).

Results further illustrate the spatio-temporal variability in reservoir construction across Mainland Southeast Asia. After 2017, all basins – except for the Lower Mekong – reached a plateau, with no significantly increasing trends in their aggregated

340   reservoir storage (Fig. 6). For instance, 1998-2015 was the period in which a series of reservoirs were constructed in the Irrawaddy basin, increasing the aggregated storage volume form ~2 km^3 to 10 km^3 (500% increase). Similarly, it was in 2005-2015 and 2010-2017, respectively, that the largest reservoirs were built in Red river (300% increase) and in the other-coastal basins (35% increase) (Fig. 6c, f). The aggregated reservoir storage in the Lower Mekong basin has instead increased since 2009 (Fig. 6g). Two river basins – Salwaeen and Chao Phraya – show no significant change in the aggregated reservoir storage

345   in last four decades (Fig. 6d, e). In fact, the storage volume in Chao Phraya has slightly decreased (~15%) in the post-2010 period (Fig. 6e). Putting all 185 reservoirs all together, we find that the aggregated average reservoir storage in Mainland Southeast Asia has increased significantly, from 70 to 160 km^3 (130% increase), during the period 2008-2017. Presently, it is approximately 175 km^3 (Fig. 6h). Additional details regarding the temporal evolution of reservoir storage in MSEA are reported in Fig. S1.

350
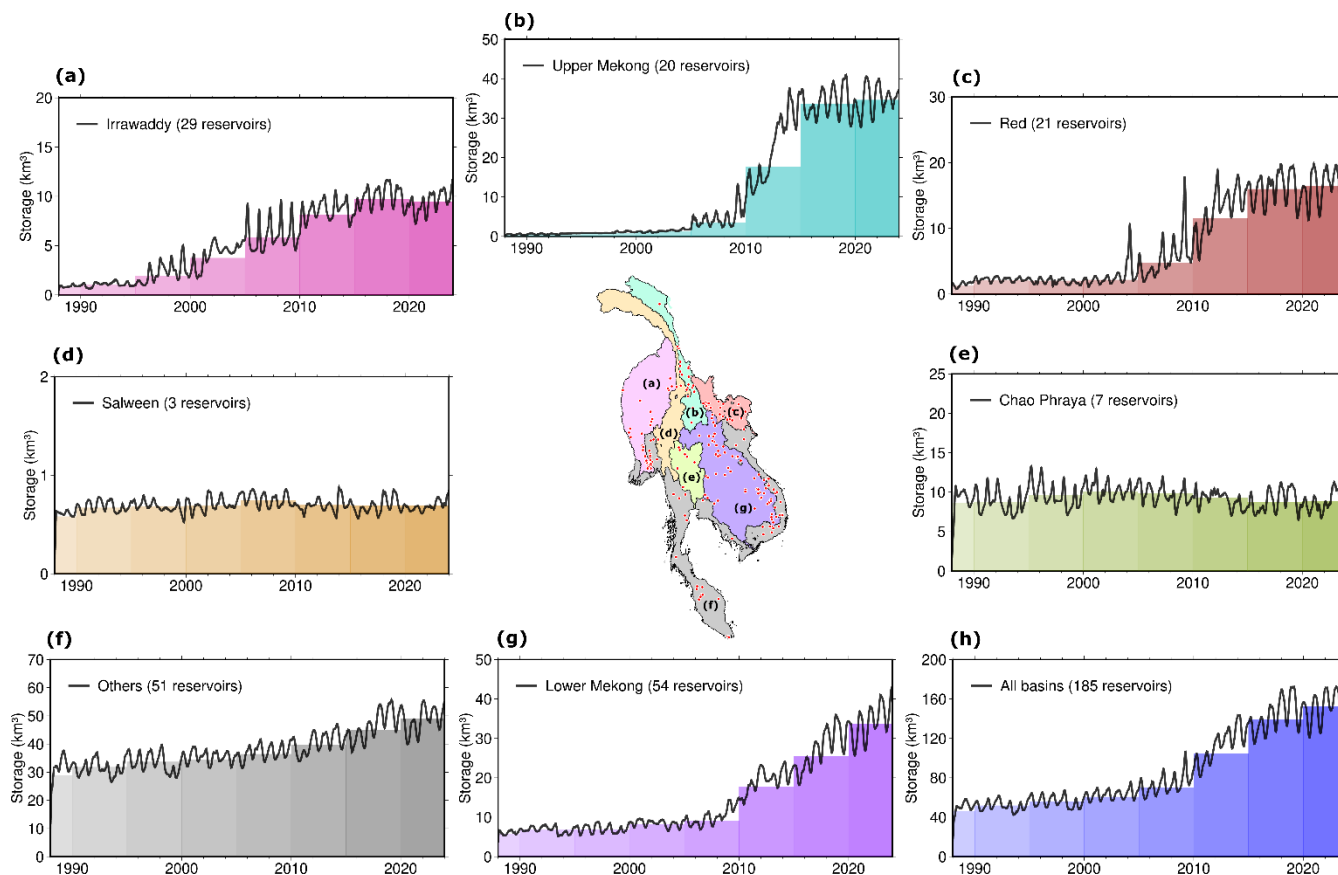
Figure 6: (a-g) Aggregated storage time series in Irrawaddy, Upper Mekong, Red, Salween, Chao Phraya, Lower Mekong and other minor river basins, during the 1985-2023 period. (h) Aggregated storage time series of all the 185 reservoirs in Mainland

355 **Southeast Asia. The color gradient in each panel represents the average storage with a 5-year interval. Please note that the aggregated storage is the total volume of water (km³) stored in all reservoirs at a given time in each river basin.**

4.4 Validation

We validated the generated storage time series – Level-1 data – with the observed reservoir storage (direct validation) and altimetry-converted storage (indirect validation). As explained in Section 3.4, we first collected observed storage for 20

360 reservoirs in Thailand from the National Water Database, the only publicly available storage database in the MSEA region. We then compared the estimated and observed storage based on two metrics – coefficient of determination (R^2) and normalized (by reservoir's total storage) root-mean-square-error (nRMSE).

Despite the lack of actual bathymetry for most reservoirs in Thailand (since they were built before 2000), we found a good

365 agreement between estimated and directly observed storage in most reservoirs (Fig. 7a, b). Sirikit and Shringarind showed

very good agreement, with $R^2 > 0.8$ and nRMSE < 9.5% for both reservoirs (Fig. 7c, d). Notably, 10 out of 20 reservoirs show an R^2 greater than 0.7 (average $R^2 = 0.77$ and average nRMSE = 14.2%) (Fig. 7a, b; Table S1). Excluding three reservoirs with lower performances (Bang Lang, Rajjaprabha, and Bhumibol), the average R^2 and nRMSE of the remaining 17 reservoirs is 0.68 and 17%, respectively (Table S1), suggesting that the framework works well for reservoirs characterized by different A-E-S curves and sizes. For instance, the validation shows a considerably good agreement for both Khao Laem (~8 km^3) and Lamphraphloeng (~0.1 km^3), with $R^2 > 0.77$ and nRMSE < 18% for both reservoirs (Fig. S3, Table S1).

To make the evaluation more robust, we indirectly validated our storage time series using altimeter observations collected from the DAHITI and G-REALM databases. The water level time series acquired from various altimeters was converted to the corresponding storage-time series using the Elevation-Storage (E-S) curve (see Section 3.4). We collected water level observations for 20 reservoirs across the MSEA region for which the altimetry passes were available for at least five years. The comparison between time series shows that 14 of 20 reservoirs have an R^2 larger than 0.7 (average $R^2 = 0.80$ and average nRMSE = 11.7%), suggesting a good match between estimated and altimetry-converted storage time series (Fig. 8a, b). The average R^2 and nRMSE are 0.63 and 13.3%, respectively, when considering all 20 reservoirs together (Table S2). The storage time series comparison for two of the largest reservoirs [Sirikit ($R^2 = 0.70$, nRMSE = 17%)] and Nuozhadu [($R^2 = 0.96$, nRMSE = 6.4%)] are shown in Fig. 8c and Fig. 8d, respectively. Overall, the direct and indirect validation metrics suggest that the *InfeRes*-derived storage data can be reliably used for water storage-related analysis on a weekly to yearly time scale.
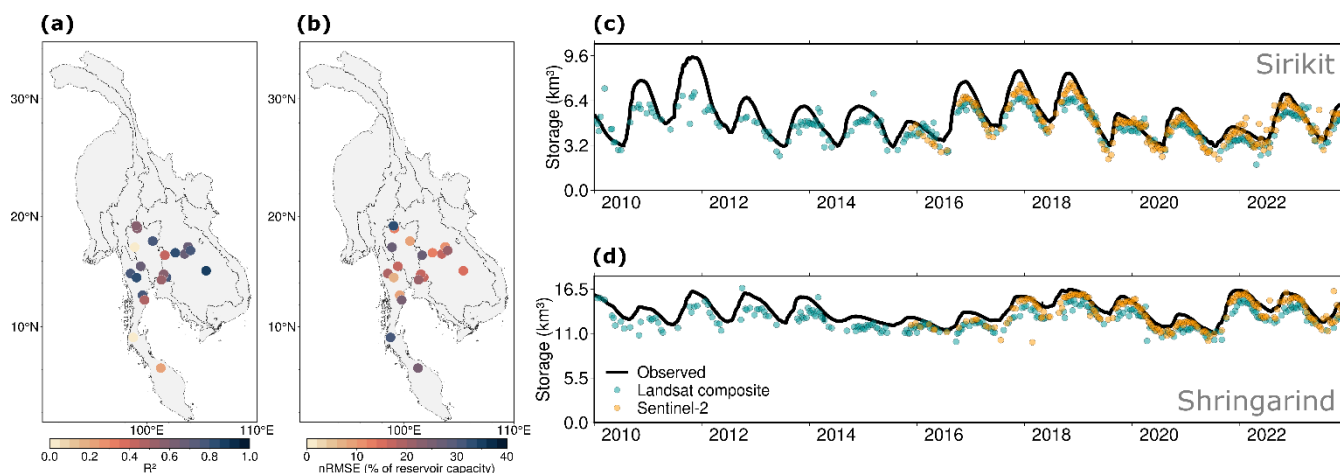
Figure 7: Direct validation of the inferred storage time series against local observations. (a-b) Spatial distribution of the coefficient of determination (R^2) and nRMSE, respectively. (c) Comparison of the absolute storage time series for Sirikit reservoir during the period 2010-2023. (d) Same as (c), but for Shringarind reservoir.
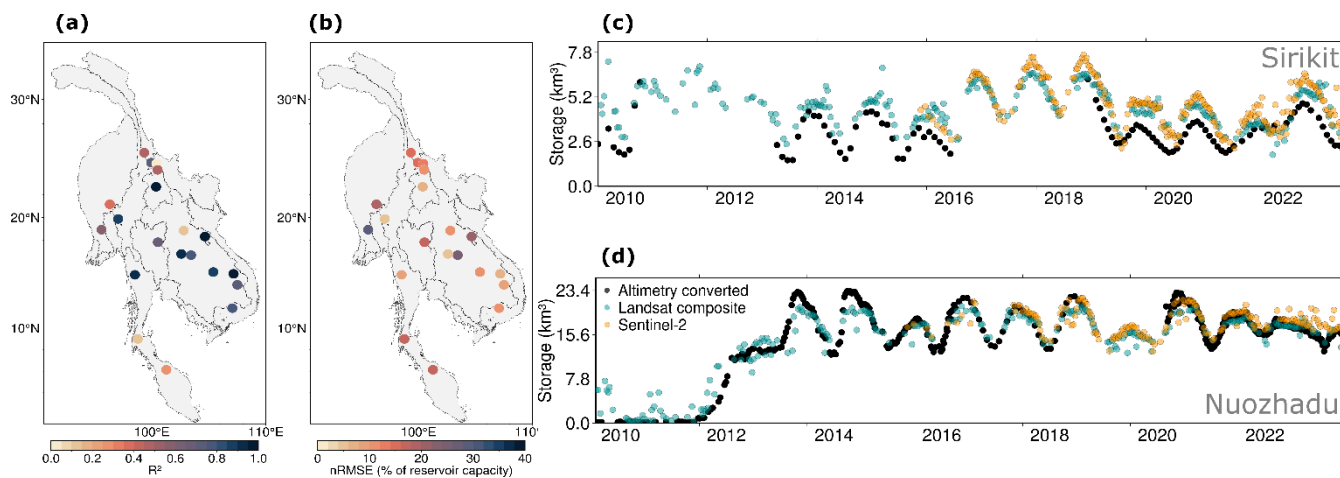
390

Figure 8: Indirect validation of the inferred storage time series against the altimetry-converted storage (water level is converted to the corresponding storage using the Elevation-Storage curve). (a-b) Spatial distribution of the coefficient of determination (R^2) and nRMSE, respectively. (c) Comparison of the absolute storage time series for Sirikit reservoir during the period 2010-2023. (d) Same as (c), but for Nuozhadu reservoir.

4.5 Example application: 2019-2020 drought's impact on water storage

395

We finally used the estimated storage time series (Level-1 data) to showcase an example application of the MSEA-Res database. Studies reported that the 2019-2020 drought in the MSEA region seriously impacted agriculture, water resources, and hydropower generation (Ha et al., 2022, 2023). Banking on the new developed data, we analysed the impact of the 2019-2020 drought on surface water storage across the region by utilizing precipitation data from the Climate Hazards group Infrared

400 Precipitation with Stations [CHIRPS; (Funk et al., 2015)] and storage anomalies for all 185 reservoirs.

The precipitation anomalies (%) in 2019 and 2020 with respect to the reference period 1981-2023 are very pronounced (Fig. 9a and 9b). In 2019, Mainland Southeast Asia experienced wide-spread below-average precipitation conditions, with rainfall significantly lower than the historical average in most areas, with some regions facing a decrease as high as -40% (Fig. 9a).

405 Nearly 30% of the MSEA region suffered from more than five months of drought, impacting, in particular, Cambodia and Thailand (Fig. 9a). In contrast, 2020 showed a more mixed pattern, with several areas experiencing above-average precipitation while others continuing to have below-average levels (Fig. 9b). Overall, these severe drought conditions damaged nearly 40% of the rainfed rice area (Ha et al., 2023) and also threatened the surface water storage in lakes and reservoirs (ReliefWeb report, 2020; Ha et al., 2022).

410

To quantify the impact of the drought on the reservoir's storage volume, we estimated the reservoir storage anomalies in 2019 and 2020 against the reference period 2017-2023. The anomalies in storage volume of the selected reservoirs for 2019 and

2020 are mostly negative (Fig. 9c and 9d). In 2019, 120 of 185 reservoirs (65%) exhibited negative storage departures, reflecting reduced water levels consistent with the observed precipitation deficit (Fig. 9c). These storage departures ranged up to -40%, highlighting significant impacts on water availability in the region. Many lakes in Cambodia and Thailand were indeed hardly hit by drought conditions, resulting in below-average levels. Reservoirs situated in the eastern basins (e.g., Mekong, Red river) were affected the most, compared to the reservoirs in the western part, where some reservoirs showed positive storage anomalies (Fig. 9c). Storage conditions worsened even further in 2020, with 144 of 185 reservoirs (78%) exhibiting negative storage departures, primarily due to the combined effects of precipitation deficits in both 2019 and 2020 (Fig. 9d). Except for reservoirs in the Upper Mekong basin, all other reservoirs experienced storage anomalies ranging between -5% to -40% (Fig. 9d). This is in line with direct observations, as the reservoirs in nine provinces of Thailand -- Chiang Mai, Uthai Thani, Chaiyaphum, Khon Kaen, Nakhon Ratchasima, Buri Ram, Suphan Buri, Lop Buri, and Chachoengsao – were reported to reach low storage values (ReliefWeb report, 2020; Danial R, 2021). As a result, Thailand experienced the worst water crisis in the past 40 years, with 25 provinces declaring drought disaster zones (Danial R., 2021). Moreover, the 2019-2020 water shortage increased the political tensions among countries, particularly in the Upper-Mekong Region, since China was criticized for holding back water in its dams, thus exacerbating the impact of the drought in the lower basins. Overall, analyses like this one illustrate the importance of working with detailed information on reservoir operations when analysing the impact of droughts: aside from the preliminary analysis reported here, one could, for instance combine the storage data with a hydrological model to investigate the drought impact on the Mekong level, which was reported to have reached the lowest level in almost 100 years (MRC report, 2020).
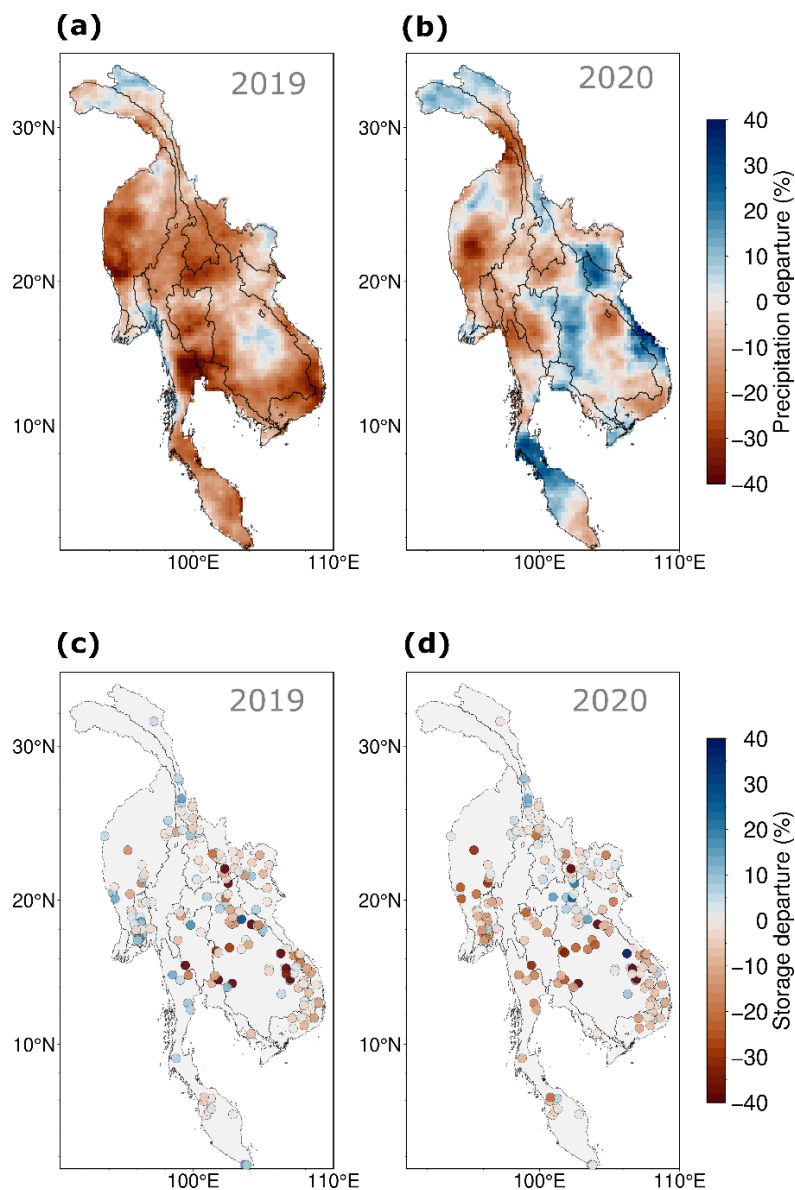
Figure 9: Precipitation and water storage anomalies during the 2019-2020 drought in Mainland Southeast Asia. (a-b) Spatial variability in the precipitation anomalies (%) in 2019 and 2020. (c-d) Same as (a-b), but for reservoir storage anomalies. The anomalies of precipitation were estimated against the reference period 1985-2023, whereas, for storage anomalies, the reference period is 2017-2023.

435

5 Conclusions

We produced time series of absolute storage for 185 reservoirs (with capacity larger than 0.1 km^3) in Mainland Southeast Asia for the period 1985-2023 with an aggregated storage capacity of nearly 175 km³, which corresponds to about 60 mm of water storage over the entire mainland Southeast Asia region. The reservoir time series were reconstructed using optical remote
440 sensing data (NDWI) from Landsat composite and Sentinel-2 with a 10-day temporal resolution. The reservoir locations and other attributes, such as design capacity, year of commission, and maximum surface area, were retrieved by combining GRanD v1.3, the Mekong Dam database (Ang et al., (2024)), and the GDAT database. For each reservoir, we generated (i) scene-based NDWI raster image, (ii) water frequency raster, (iii) maximum water extent raster, and (iv) elevation raster (i.e., DEM). A Python package called '*InfeRes*' was created to automatically download and process all satellite images using the Google Earth
445 Engine Python API. The water area from the satellite data was then translated into storage values using hypsometric curves (Area-Elevation-Storage relationship) derived from the SRTM Digital Elevation Model (DEM) and bathymetry reconstructions from the GRDL database, wherever necessary.

The reconstructed database of absolute storage time series – unlike storage change metrics – offers a detailed view of reservoir
450 status at any given time, thus providing a comprehensive and contextualized understanding of reservoir dynamics. This approach is particularly valuable for long-term monitoring (Gao et al., 2012) and planning of water resources in the region (Galelli et al., 2022; Minocha et al., 2024). Accurate absolute storage estimates allow for detecting subtle trends and shifts in water availability that could be masked by focusing solely on changes (Hou et al., 2024; Li et al., 2023). This is particularly crucial for transboundary rivers like the Mekong, where the availability of data on reservoir operations could help alleviate the
455 water governance issues that emerged in the past years (Danial R., 2021). Another important downstream application of MSEA-Res is hydrological modelling; integrating the estimated absolute reservoir storage data into hydrological models can offer significant advances in the understanding of human-water interactions and resource management in Mainland Southeast Asia. This integration allows for refining models that simulate water management strategies (Chang et al., 2019; Chowdhury et al., 2020; Galelli et al., 2022), flood control (Shin et al., 2020; Wang et al., 2021).

460

Although the extraction of water surface area using optical images from Landsat and Sentinel-2 has provided valuable insights, there remains scope for further improvements. One opportunity lies in the integration of Sentinel-1 SAR data. Unlike optical sensors, Sentinel-1 SAR can penetrate clouds and operate under all weather conditions, offering consistent and reliable observations. The higher spatial resolution of Sentinel data (10 m) compared to Landsat (30 m) also enables more accurate
465 classification of water and non-water pixels. Looking ahead, storage estimates can be further improved by combining Sentinel-1's microwave SAR data with observations from the recently operational NASA SWOT mission (https://swot.jpl.nasa.gov/), which provides a wide coverage of water height measurements (Altenau et al., 2021; Hausman et al., 2021; Hossain et al.,

2022). This integration would not only enhance the detection and classification of water bodies but also allow for a more precise estimation of reservoir storage by linking surface area with accurate water height data.

470

Importantly, the developed code (available at https://doi.org/10.5281/zenodo.12787699) and framework are not tailored to Southeast Asia, therefore enabling their application to individual studies or other regions as well as further enrichment of this inventory with new reservoirs. The publicly available reservoir time series dataset can be used directly to assess storage trends and variability under climate change, inferring reservoir operations, agricultural water management, and hydrological model's

475 inputs, and for comparison with previous studies. The overall outcome of our study will hopefully facilitate reservoir management and related research in hydrology, environmental science, and climate studies.

6 Data and code availability

The raw satellite data used in this study were acquired from Google Earth's engine. The reservoir location information was collected from the GRanD database (Lehner et al., 2011- https://esajournals.onlinelibrary.wiley.com/doi/abs/10.1890/100125),

480 the Mekong database (Ang et al., 2024- https://essd.copernicus.org/articles/16/1209/2024/), and the GDAT database (Zhang and Gu, 2023- https://www.nature.com/articles/s41597-023-02008-2), which are all publicly available. The supporting data – reconstructed reservoir bathymetry – were collected from the GRDL database (Hao et al., 2024), publicly available at https://agupubs.onlinelibrary.wiley.com/doi/full/10.1029/2023WR035781. The MSEA-Res database containing the absolute reservoir storage time series and Python code are available at https://doi.org/10.5281/zenodo.12787699 (Mahto et al., 2024).

485 **Author contribution**

S.S.M., S.G., and S.F. have conceived the idea and acquired the funds. S.S.M. developed the methodology and software, conducted the investigation and analysis, curated the data, and drafted the initial manuscript. S.G., S.F., and F.H. reviewed and edited the manuscript.

Competing interests

490 The contact author has declared that none of the authors has any competing interests.

Acknowledgments

This work is funded by the Singapore's Ministry of Education (MoE) under its Academic Research Fund Tier 2, Project ID: MOE-000379-00/MOE-000379-01, Award Number: MOE-T2EP50122-0004. We thank NUS Singapore for providing the

technical resources and infrastructure to conduct the research. We also thank Prof. Faisal Hossain for his suggestions at the
495   initial stages of this study.

References

Altenau, E. H., Pavelsky, T. M., Durand, M. T., Yang, X., Frasson, R. P. de M., and Bendezu, L.: The Surface Water and Ocean Topography (SWOT) Mission River Database (SWORD): A Global River Network for Satellite Data Products, Water Resources Research, 57, e2021WR030054, https://doi.org/10.1029/2021WR030054, 2021.

500   Ang, W. J., Park, E., Pokhrel, Y., Tran, D. D., and Loc, H. H.: Dams in the Mekong: a comprehensive database, spatiotemporal distribution, and hydropower potentials, Earth System Science Data, 16, 1209–1228, https://doi.org/10.5194/essd-16-1209-2024, 2024.

Weekly Dry Season Situation Report for the Mekong River Basin - Prepared on: 03/12/2019, covering the week from 26th November to 2nd December 2019 - World | ReliefWeb: https://reliefweb.int/report/world/weekly-dry-season-situation-report-
505   mekong-river-basin-prepared-03122019-covering-week, last access: 21 July 2024.

Southeast Asia: Drought - 2019-2020 | ReliefWeb: https://reliefweb.int/disaster/dr-2019-000113-phl, last access: 20 July 2024.

Dams and droughts, data and diplomacy in the Mekong: https://www.sei.org/perspectives/dams-and-droughts-data-and-diplomacy-in-the-mekong/, last access: 20 July 2024a.

Dams and droughts, data and diplomacy in the Mekong: https://www.sei.org/perspectives/dams-and-droughts-data-and-
510   diplomacy-in-the-mekong/, last access: 20 July 2024b.

Bacalhau, J. R., Ribeiro Neto, A., Crétaux, J.-F., Bergé-Nguyen, M., and Moreira, D. M.: Bathymetry of reservoirs using altimetric data associated to optical images, Advances in Space Research, 69, 4098–4110, https://doi.org/10.1016/j.asr.2022.03.011, 2022.

Bakken, T. H., Aase, A. G., Hagen, D., Sundt, H., Barton, D. N., and Lujala, P.: Demonstrating a new framework for the
515   comparison of environmental impacts from small- and large-scale hydropower and wind power projects, Journal of Environmental Management, 140, 93–101, https://doi.org/10.1016/j.jenvman.2014.01.050, 2014.

Birkett, C., Reynolds, C., Beckley, B., and Doorn, B.: From Research to Operations: The USDA Global Reservoir and Lake Monitor, in: Coastal Altimetry, edited by: Vignudelli, S., Kostianoy, A. G., Cipollini, P., and Benveniste, J., Springer, Berlin, Heidelberg, 19–50, https://doi.org/10.1007/978-3-642-12796-0_2, 2011.

520   Birkett, C. M.: Contribution of the TOPEX NASA Radar Altimeter to the global monitoring of large rivers and wetlands, Water Resources Research, 34, 1223–1239, https://doi.org/10.1029/98WR00124, 1998.

Busker, T., de Roo, A., Gelati, E., Schwatke, C., Adamovic, M., Bisselink, B., Pekel, J.-F., and Cottam, A.: A global lake and reservoir volume analysis using a surface water dataset and satellite altimetry, Hydrology and Earth System Sciences, 23, 669–690, https://doi.org/10.5194/hess-23-669-2019, 2019.

525   Chang, J., Guo, A., Wang, Y., Ha, Y., Zhang, R., Xue, L., and Tu, Z.: Reservoir Operations to Mitigate Drought Effects With a Hedging Policy Triggered by the Drought Prevention Limiting Water Level, Water Resources Research, 55, 904–922, https://doi.org/10.1029/2017WR022090, 2019.

Chao, B. F., Wu, Y. H., and Li, Y. S.: Impact of artificial reservoir water impoundment on global sea level, Science, 320, 212–214, https://doi.org/10.1126/science.1154580, 2008.

530 Chen, T., Song, C., Luo, S., Ke, L., Liu, K., and Zhu, J.: Monitoring global reservoirs using ICESat-2: Assessment on spatial coverage and application potential, Journal of Hydrology, 604, 127257, https://doi.org/10.1016/j.jhydrol.2021.127257, 2022.

Chowdhury, A. F. M. K., Dang, T. D., Bagchi, A., and Galelli, S.: Expected Benefits of Laos' Hydropower Development Curbed by Hydroclimatic Variability and Limited Transmission Capacity: Opportunities to Reform, Journal of Water Resources Planning and Management, 146, 05020019, https://doi.org/10.1061/(ASCE)WR.1943-5452.0001279, 2020.

535 Cooley, S. W., Ryan, J. C., and Smith, L. C.: Human alteration of global surface water storage variability, Nature, 591, 78–81, https://doi.org/10.1038/s41586-021-03262-3, 2021.

Crétaux, J.-F., Arsen, A., Calmant, S., Kouraev, A., Vuglinski, V., Bergé-Nguyen, M., Gennero, M.-C., Nino, F., Abarca Del Rio, R., Cazenave, A., and Maisongrande, P.: SOLS: A lake database to monitor in the Near Real Time water level and storage variations from remote sensing data, Advances in Space Research, 47, 1497–1507, https://doi.org/10.1016/j.asr.2011.01.004,
540 2011.

Dang, T. D., Chowdhury, A. F. M. K., and Galelli, S.: On the representation of water reservoir storage and operations in large-scale hydrological models: implications on model parameterization and climate change impact assessments, Hydrology and Earth System Sciences, 24, 397–416, https://doi.org/10.5194/hess-24-397-2020, 2020.

Das, P., Hossain, F., Khan, S., Biswas, N. K., Lee, H., Piman, T., Meechaiya, C., Ghimire, U., and Hosen, K.: Reservoir
545 Assessment Tool 2.0: Stakeholder driven improvements to satellite remote sensing based reservoir monitoring, Environmental Modelling & Software, 157, 105533, https://doi.org/10.1016/j.envsoft.2022.105533, 2022.

Degu, A. M., Hossain, F., Niyogi, D., Pielke Sr., R., Shepherd, J. M., Voisin, N., and Chronis, T.: The influence of large dams on surrounding climate and precipitation patterns, Geophysical Research Letters, 38, https://doi.org/10.1029/2010GL046482, 2011.

550 Fang, C., Lu, S., Li, M., Wang, Y., Li, X., Tang, H., and Odion Ikhumhen, H.: Lake water storage estimation method based on similar characteristics of above-water and underwater topography, Journal of Hydrology, 618, 129146, https://doi.org/10.1016/j.jhydrol.2023.129146, 2023.

Farr, T. G., Rosen, P. A., Caro, E., Crippen, R., Duren, R., Hensley, S., Kobrick, M., Paller, M., Rodriguez, E., Roth, L., Seal, D., Shaffer, S., Shimada, J., Umland, J., Werner, M., Oskin, M., Burbank, D., and Alsdorf, D.: The Shuttle Radar Topography
555 Mission, Reviews of Geophysics, 45, https://doi.org/10.1029/2005RG000183, 2007.

Frappart, F., Calmant, S., Cauhopé, M., Seyler, F., and Cazenave, A.: Preliminary results of ENVISAT RA-2-derived water levels validation over the Amazon basin, Remote Sensing of Environment, 100, 252–264, https://doi.org/10.1016/j.rse.2005.10.027, 2006.

Funk, C., Peterson, P., Landsfeld, M., Pedreros, D., Verdin, J., Shukla, S., Husak, G., Rowland, J., Harrison, L., Hoell, A., and
560 Michaelsen, J.: The climate hazards infrared precipitation with stations—a new environmental record for monitoring extremes, Sci Data, 2, 150066, https://doi.org/10.1038/sdata.2015.66, 2015.

Galelli, S., Dang, T. D., Ng, J. Y., Chowdhury, A. F. M. K., and Arias, M. E.: Opportunities to curb hydrological alterations via dam re-operation in the Mekong, Nat Sustain, 5, 1058–1069, https://doi.org/10.1038/s41893-022-00971-z, 2022.

Gao, H., Birkett, C., and Lettenmaier, D. P.: Global monitoring of large reservoir storage from satellite remote sensing, Water
565 Resources Research, 48, https://doi.org/10.1029/2012WR012063, 2012.

Ha, T. V., Huth, J., Bachofer, F., and Kuenzer, C.: A Review of Earth Observation-Based Drought Studies in Southeast Asia,
Remote Sensing, 14, 3763, https://doi.org/10.3390/rs14153763, 2022.

Ha, T. V., Uereyen, S., and Kuenzer, C.: Agricultural drought conditions over mainland Southeast Asia: Spatiotemporal
characteristics revealed from MODIS-based vegetation time-series, International Journal of Applied Earth Observation and
570 Geoinformation, 121, 103378, https://doi.org/10.1016/j.jag.2023.103378, 2023.

Haddeland, I., Heinke, J., Biemans, H., Eisner, S., Flörke, M., Hanasaki, N., Konzmann, M., Ludwig, F., Masaki, Y., Schewe,
J., Stacke, T., Tessler, Z. D., Wada, Y., and Wisser, D.: Global water resources affected by human interventions and climate
change, Proceedings of the National Academy of Sciences, 111, 3251–3256, https://doi.org/10.1073/pnas.1222475110, 2014.

Hao, Z., Chen, F., Jia, X., Cai, X., Yang, C., Du, Y., and Ling, F.: GRDL: A New Global Reservoir Area-Storage-Depth Data
575 Set Derived Through Deep Learning-Based Bathymetry Reconstruction, Water Resources Research, 60, e2023WR035781,
https://doi.org/10.1029/2023WR035781, 2024.

Hausman, J., Moroni, D., Gangl, M., Zlotnicki, V., Vazquez-Cuervo, J., Armstrong, E. M., Oaida, C., Gierach, M., Finch, C.,
and Schroeder, C.: The evolution of the PO.DAAC: Seasat to SWOT, Advances in Space Research, 68, 1187–1193,
https://doi.org/10.1016/j.asr.2019.11.030, 2021.

580 Hossain, F., Das, P., Srinivasan, M., Tsontos, V., Oaida, C. M., Nickles, C., McNelis, J., Bonnema, M., Picot, N., Peña-Luque,
S., Doorn, B., Vinogradova-Shiffer, N., Andral, A., Gaultier, L., Jayaluxmi, I., Zhu, J., Fernando, N., Ul-Hasan, F., Fatima,
B., Ahsan, M., Dhanya, C. T., Jayasinghe, S., Meechaiya, C., Barajas, M., Balakrishnan, V., Eldardiry, H., Elkholy, M.,
Abdelrazek, A., Fenoglio, L., Durand, M., Wei, R., and Pavelsky, T.: Building User-Readiness for Satellite Earth Observing
Missions: The Case of the Surface Water and Ocean Topography (SWOT) Mission, AGU Advances, 3, e2022AV000680,
585 https://doi.org/10.1029/2022AV000680, 2022.

Hou, J., Van Dijk, A. I. J. M., Renzullo, L. J., and Larraondo, P. R.: GloLakes: water storage dynamics for 27 000
lakes globally from 1984 to present derived from satellite altimetry and optical imaging, Earth System Science Data, 16, 201–
218, https://doi.org/10.5194/essd-16-201-2024, 2024.

Khazaei, B., Read, L. K., Casali, M., Sampson, K. M., and Yates, D. N.: GLOBathy, the global lakes bathymetry dataset, Sci
590 Data, 9, 36, https://doi.org/10.1038/s41597-022-01132-9, 2022.

Kirchherr, J., Pohlner, H., and Charles, K. J.: Cleaning up the big muddy: A meta-synthesis of the research on the social impact
of dams, Environmental Impact Assessment Review, 60, 115–125, https://doi.org/10.1016/j.eiar.2016.02.007, 2016.

Lehner, B., Liermann, C. R., Revenga, C., Vörösmarty, C., Fekete, B., Crouzet, P., Döll, P., Endejan, M., Frenken, K.,
Magome, J., Nilsson, C., Robertson, J. C., Rödel, R., Sindorf, N., and Wisser, D.: High-resolution mapping of the world's
595 reservoirs and dams for sustainable river-flow management, Frontiers in Ecology and the Environment, 9, 494–502,
https://doi.org/10.1890/100125, 2011.

Li, Y., Gao, H., Zhao, G., and Tseng, K.-H.: A high-resolution bathymetry dataset for global reservoirs using multi-source
satellite imagery and altimetry, Remote Sensing of Environment, 244, 111831, https://doi.org/10.1016/j.rse.2020.111831,
2020.

600 Li, Y., Zhao, G., Allen, G. H., and Gao, H.: Diminishing storage returns of reservoir construction, Nat Commun, 14, 3203,
https://doi.org/10.1038/s41467-023-38843-5, 2023.

Liu, K. and Song, C.: Modeling lake bathymetry and water storage from DEM data constrained by limited underwater surveys, Journal of Hydrology, 604, 127260, https://doi.org/10.1016/j.jhydrol.2021.127260, 2022.

605 Liu, K., Song, C., Wang, J., Ke, L., Zhu, Y., Zhu, J., Ma, R., and Luo, Z.: Remote Sensing-Based Modeling of the Bathymetry and Water Storage for Channel-Type Reservoirs Worldwide, Water Resources Research, 56, e2020WR027147, https://doi.org/10.1029/2020WR027147, 2020.

Maavara, T., Chen, Q., Van Meter, K., Brown, L. E., Zhang, J., Ni, J., and Zarfl, C.: River dam impacts on biogeochemical cycling, Nat Rev Earth Environ, 1, 103–116, https://doi.org/10.1038/s43017-019-0019-0, 2020.

Mahto, S. S., Galelli, S., and Fatichi, S.: A comprehensive time series dataset of absolute reservoir storage in Mainland 610 Southeast Asia (MSEA-Res) from 1985 to 2023, https://doi.org/10.5281/zenodo.12787699, 2024.

Markert, K. N., Pulla, S. T., Lee, H., Markert, A. M., Anderson, E. R., Okeowo, M. A., and Limaye, A. S.: AltEx: An open source web application and toolkit for accessing and exploring altimetry datasets, Environmental Modelling & Software, 117, 164–175, https://doi.org/10.1016/j.envsoft.2019.03.021, 2019.

McFEETERS, S. K.: The use of the Normalized Difference Water Index (NDWI) in the delineation of open water features, 615 International Journal of Remote Sensing, 17, 1425–1432, https://doi.org/10.1080/01431169608948714, 1996.

Messager, M. L., Lehner, B., Grill, G., Nedeva, I., and Schmitt, O.: Estimating the volume and age of water stored in global lakes using a geo-statistical approach, Nat Commun, 7, 13603, https://doi.org/10.1038/ncomms13603, 2016.

Minocha, S., Hossain, F., Das, P., Suresh, S., Khan, S., Darkwah, G., Lee, H., Galelli, S., Andreadis, K., and Oddo, P.: Reservoir Assessment Tool version 3.0: a scalable and user-friendly software platform to mobilize the global water 620 management community, Geoscientific Model Development, 17, 3137–3156, https://doi.org/10.5194/gmd-17-3137-2024, 2024.

Nazemi, A. and Wheater, H. S.: On inclusion of water resource management in Earth system models – Part 1: Problem definition and representation of water demand, Hydrology and Earth System Sciences, 19, 33–61, https://doi.org/10.5194/hess-19-33-2015, 2015a.

625 Nazemi, A. and Wheater, H. S.: On inclusion of water resource management in Earth system models – Part 2: Representation of water supply and allocation and opportunities for improved modeling, Hydrology and Earth System Sciences, 19, 63–90, https://doi.org/10.5194/hess-19-63-2015, 2015b.

Nguyen, H. T. T., Turner, S. W. D., Buckley, B. M., and Galelli, S.: Coherent Streamflow Variability in Monsoon Asia Over the Past Eight Centuries—Links to Oceanic Drivers, Water Resources Research, 56, e2020WR027883, 630 https://doi.org/10.1029/2020WR027883, 2020.

Reza, A. M.: Realization of the Contrast Limited Adaptive Histogram Equalization (CLAHE) for Real-Time Image Enhancement, The Journal of VLSI Signal Processing-Systems for Signal, Image, and Video Technology, 38, 35–44, https://doi.org/10.1023/B:VLSI.0000028532.53893.82, 2004.

Santos da Silva, J., Calmant, S., Seyler, F., Rotunno Filho, O. C., Cochonneau, G., and Mansur, W. J.: Water levels in the 635 Amazon basin derived from the ERS 2 and ENVISAT radar altimetry missions, Remote Sensing of Environment, 114, 2160–2181, https://doi.org/10.1016/j.rse.2010.04.020, 2010.

Schwatke, C., Dettmering, D., Bosch, W., and Seitz, F.: DAHITI – an innovative approach for estimating water level time series over inland waters using multi-mission satellite altimetry, Hydrology and Earth System Sciences, 19, 4345–4364, https://doi.org/10.5194/hess-19-4345-2015, 2015.

640 Shen, Y., Liu, D., Jiang, L., Nielsen, K., Yin, J., Liu, J., and Bauer-Gottwein, P.: High-resolution water level and storage variation datasets for 338 reservoirs in China during 2010–2021, Earth System Science Data, 14, 5671–5694, https://doi.org/10.5194/essd-14-5671-2022, 2022.

Shen, Y., Nielsen, K., Revel, M., Liu, D., and Yamazaki, D.: Res-CN (Reservoir dataset in China): hydrometeorological time series and landscape attributes across 3254 Chinese reservoirs, Earth System Science Data, 15, 2781–2808, 645 https://doi.org/10.5194/essd-15-2781-2023, 2023.

Shin, S., Pokhrel, Y., Yamazaki, D., Huang, X., Torbick, N., Qi, J., Pattanakiat, S., Ngo-Duc, T., and Nguyen, T. D.: High Resolution Modeling of River-Floodplain-Reservoir Inundation Dynamics in the Mekong River Basin, Water Resources Research, 56, e2019WR026449, https://doi.org/10.1029/2019WR026449, 2020.

Skliris, N., Marsh, R., Haigh, I. D., Wood, M., Hirschi, J., Darby, S., Quynh, N. P., and Hung, N. N.: Drivers of rainfall trends 650 in and around Mainland Southeast Asia, Frontiers in Climate, 4, https://doi.org/10.3389/fclim.2022.926568, 2022.

Song, C., Fan, C., Zhu, J., Wang, J., Sheng, Y., Liu, K., Chen, T., Zhan, P., Luo, S., Yuan, C., and Ke, L.: A comprehensive geospatial database of nearly 100 000 reservoirs in China, Earth System Science Data, 14, 4017–4034, https://doi.org/10.5194/essd-14-4017-2022, 2022.

Tortini, R., Noujdina, N., Yeo, S., Ricko, M., Birkett, C. M., Khandelwal, A., Kumar, V., Marlier, M. E., and Lettenmaier, D. 655 P.: Satellite-based remote sensing data set of global surface water storage change from 1992 to 2018, Earth System Science Data, 12, 1141–1151, https://doi.org/10.5194/essd-12-1141-2020, 2020.

Vörösmarty, C. J., McIntyre, P. B., Gessner, M. O., Dudgeon, D., Prusevich, A., Green, P., Glidden, S., Bunn, S. E., Sullivan, C. A., Liermann, C. R., and Davies, P. M.: Global threats to human water security and river biodiversity, Nature, 467, 555–561, https://doi.org/10.1038/nature09440, 2010.

660 Vu, D. T., Dang, T. D., Galelli, S., and Hossain, F.: Satellite observations reveal 13 years of reservoir filling strategies, operating rules, and hydrological alterations in the Upper Mekong River basin, Hydrology and Earth System Sciences, 26, 2345–2364, https://doi.org/10.5194/hess-26-2345-2022, 2022.

Wada, Y., Bierkens, M. F. P., de Roo, A., Dirmeyer, P. A., Famiglietti, J. S., Hanasaki, N., Konar, M., Liu, J., Müller Schmied, H., Oki, T., Pokhrel, Y., Sivapalan, M., Troy, T. J., van Dijk, A. I. J. M., van Emmerik, T., Van Huijgevoort, M. H. J., Van 665 Lanen, H. A. J., Vörösmarty, C. J., Wanders, N., and Wheater, H.: Human–water interface in hydrological modelling: current status and future directions, Hydrology and Earth System Sciences, 21, 4169–4193, https://doi.org/10.5194/hess-21-4169-2017, 2017.

Wang, J., Yun, X., Pokhrel, Y., Yamazaki, D., Zhao, Q., Chen, A., and Tang, Q.: Modeling Daily Floods in the Lancang-Mekong River Basin Using an Improved Hydrological-Hydrodynamic Model, Water Resources Research, 57, 670 e2021WR029734, https://doi.org/10.1029/2021WR029734, 2021.

Weekley, D. and Li, X.: Tracking Multidecadal Lake Water Dynamics with Landsat Imagery and Topography/Bathymetry, Water Resources Research, 55, 8350–8367, https://doi.org/10.1029/2019WR025500, 2019.

Wheeler, K. G., Basheer, M., Mekonnen, Z. T., Eltoum, S. O., Mersha, A., Abdo, G. M., Zagona, E. A., Hall, J. W., and Dadson, S. J.: Cooperative filling approaches for the Grand Ethiopian Renaissance Dam, Water International, 41, 611–634, https://doi.org/10.1080/02508060.2016.1177698, 2016.

Winemiller, K. O., McIntyre, P. B., Castello, L., Fluet-Chouinard, E., Giarrizzo, T., Nam, S., Baird, I. G., Darwall, W., Lujan, N. K., Harrison, I., Stiassny, M. L. J., Silvano, R. A. M., Fitzgerald, D. B., Pelicice, F. M., Agostinho, A. A., Gomes, L. C., Albert, J. S., Baran, E., Petrere, M., Zarfl, C., Mulligan, M., Sullivan, J. P., Arantes, C. C., Sousa, L. M., Koning, A. A., Hoeinghaus, D. J., Sabaj, M., Lundberg, J. G., Armbruster, J., Thieme, M. L., Petry, P., Zuanon, J., Vilara, G. T., Snoeks, J., Ou, C., Rainboth, W., Pavanelli, C. S., Akama, A., Soesbergen, A. V., and Sáenz, L.: Balancing hydropower and biodiversity in the Amazon, Congo, and Mekong, Science, 351, 128–129, https://doi.org/10.1126/science.aac7082, 2016.

Yigzaw, W., Li, H.-Y., Demissie, Y., Hejazi, M. I., Leung, L. R., Voisin, N., and Payn, R.: A New Global Storage-Area-Depth Data Set for Modeling Reservoirs in Land Surface and Earth System Models, Water Resources Research, 54, 10,372-10,386, https://doi.org/10.1029/2017WR022040, 2018.

Zaniolo, M., Giuliani, M., Sinclair, S., Burlando, P., and Castelletti, A.: When timing matters—misdesigned dam filling impacts hydropower sustainability, Nat Commun, 12, 3056, https://doi.org/10.1038/s41467-021-23323-5, 2021.

Zhang, A. T. and Gu, V. X.: Global Dam Tracker: A database of more than 35,000 dams with location, catchment, and attribute information, Sci Data, 10, 111, https://doi.org/10.1038/s41597-023-02008-2, 2023.

Zhang, S. and Gao, H.: Using the Digital Elevation Model (DEM) to Improve the Spatial Coverage of the MODIS Based Reservoir Monitoring Network in South Asia, Remote Sensing, 12, 745, https://doi.org/10.3390/rs12050745, 2020.

Zhang, S., Gao, H., and Naz, B. S.: Monitoring reservoir storage in South Asia from multisatellite remote sensing, Water Resources Research, 50, 8927–8943, https://doi.org/10.1002/2014WR015829, 2014.